発表者氏名	論文タイトル名	発表誌名	巻号	ページ	出版年
Sakamoto T, Oya N, Shibuya K, Nagata Y, Hiraoka M.	Dose-response relationship and dose optimization in radiotherapy of postoperative keloids.	Radiotherapy and Oncology	91(2)	271-276	2009
Matsuura K, Kimura T, Kashiwado K, Fujita K, Akagi Y, Yuki S, Murakami Y, Wadasaki K, Monzen Y, Ito A, Kagemoto M, Mori M, Ito K, Nagata Y.	Results of a preliminary study using hypofractionated involved field radiation therapy and concurrent carboplatin/paclitaxel in the treatment of locally advanced Non-Small-Cell lung cancer.	InternationalJournal of Clinical Oncology	14(5)	408-415	2009
Numasaki H, Teshima T, Shibuya H, Nishio M, Ikeda H, Ito H, Sekiguchi K, Kamikonya N, Koizumi M, Tago M, Nagata Y, Masaki H, Nishimura T, Yamada S.	National structure of radiation oncology in Japan with special reference to designated cancer care hospitals.	InternationalJournal of Clinical Oncology	14(3)	237-244	2009
Zhu SY, Mizowaki T, Norihisa Y, Takayama K, Nagata Y, Hiraoka M.	Comparisons of the impact of systematic uncertainties in patient setup and prostate motion on doses to the target among different plans for definitive external-beam radiotherapy for prostate cancer.	Int. J. Clin. Oncol.	13(1)	54-61	2008
Teshima T, Numasaki H, Shibuya H, Nishio M, Ikeda H, Ito H, Sekiguchi K, Kamikonya N, Koizumi M, Tago M, Nagata Y, Masaki H, Nishimura T, Yamada S	Japanese structure survey of radiaiton oncology in 2005 based on institutional stratification of patterns of care study.	Int. J. Radiat. Oncol. Biol. Phys.	72(1)	144-152	2008

発表者氏名	論文タイトル名	発表誌名	巻号	ページ	出版年
Norihisa Y, Nagata Y, Takayama K, Matsuo Y, Sakamoto T, Samamoto M, Mizowaki T, Yano S, Hiraoka M	Stereotactic body radiotherapy for oligometastatic lung tumors.	Int. J. Radiat. Oncol. Biol. Phys.	72(2)	398-403	2008
Chvetsov AV, Palta JJ, Nagata Y.	Time-dependent cell disintegration kinetics in lung tumors after irradiation.	Phys. Med. Biol.	53(9)	2413-2423	2008
Sanuki-Fujimoto N, SumiM, Ito Y, Imai A, Kagami Y, Sekine I, Kunitoh H, Ohe Y, Tamura T, Ikeda H.	Relation between elective nodal failure and irradiated volume in non-small-cell lung cancer(NSCLC) treated with radiotherapy using conventional fields and doses.	Radiotherapy and Oncology	91	433-437	2009
Sekine I, Sumi M, Ito Y, Tanai C, Nokihara H, Yamamoto N, Kunitoh H, Ohe Y, Tamura T.,	Gender Difference in Treatment Outcomes in Patients with Stage III Non-small Cell Lung Cancer Receiving Concurrent Chemoradiotherapy.	Jpn J Clin Oncol.	39	707-712	2009
Uno T, Sumi M, Ishihara Y, Numasaki H, Mitsumori M, Teshima T: Japanese PCS Working Subgroup of Lung Cancer.	Changes in patterns of care for limited-stage small-cell lung cancer: results of the 99-01 patterns of care study-a nationwide survey in Japan.	Int. J. Radiat. Oncol. Biol. Phys.	71	414-419	2008
Sekine I, Sumi M, Saijo N.	Local control of regional and metastatic lesions and indication for systemic chemotherapy in patients with non-small cell lung cancer.	Oncologist	13 Suppl 1	21-27	2008

発表者氏名	論文タイトル名	発表誌名	巻号	ページ	出版年
Uno T, Sumi M, et al.	Postoperative radiotherapy for non-small-cell lung cancer: results of the 1999-2001 patterns of care study nationwide process survey in Japan.	Lung Cancer	56	357-362	2007
Sekine I, Sumi M, et al.	Phase I Study of Cisplatin Analogue Nedaplatin, Paclitaxel, and Thoracic Radiotherapy for Unresectable Stage III Non-Small Cell Lung Cancer.	Jpn J Clin Oncol.	37	175-180	2007
Shimizu T, Sumi M, et al.	Concurrent Chemoradiotherapy for Limited-disease Small Cell Lung Cancer in Elderly Patients Aged 75 Years or Older.	Jpn J Clin Oncol.	37	181-185	2007
Watanabe S, and Asamura H	Lymph node dissection for lung cancer: significance, strategy, and technique.	J Thorac Oncol	4(5)	652-7	2009
Chang JW, Asamura H, Kawachi R, and Watanabe S	Gender difference in survival of resected non-small cell lung cancer: histology-related phenomenon?	J Thorac Cardiovasc Surg	137(4)	807-12	2009
Kawachi R, Watanabe S, and Asamura H	Clinicopathological characteristics of screen-detected lung cancers.	J Thorac Oncol	4(5)	615-619	2009
Kawaguchi T, Watanabe S, Kawachi R, Suzuki K, and Asamura H.	The Impact of Residual Tumor Morphology on Prognosis, Recurrence, and Fistula Formation after Lung Cancer Resection.	J. Thorac. Oncol.	3	599-603	2008

発表者氏名	論文タイトル名	発表誌名	巻号	ページ	出版年
Kawachi R, Watanabe S, Suzuki K, and Asamura H.	Clinical application of costal coaptation pins made of hydroxyapatite and poly-L-lactide composite for posterolateral thoracotomy.	Eur. J. Cardio-thoracic Surg.	34	510-513	2008
Watanabe S, Suzuki K, and Asamura H.	Superior and basal segment lung cancers in the lower lobe have different lymph node metastatic pathways and prognosis.	Ann Thorac Surg	85	1026-31	2008
Ishizumi T, Tateishi U, Watanabe S, and Matsuno Y.	Mucoepidermoid carcinoma of the lung: High-resolution CT and histopathologic findings in five cases.	Lung Cancer	60	125-131	2008
Ishizumi T, Tateishi U, Watanabe S, Maeda T, and Arai Y.	F-18 FDG PET/CT imaging of low-grade mucoepidermoid carcinoma of the bronchus.	Ann Nucl Med	21	299-302	2007
Fukui T, Tsuta T, Furuta K, Watanabe S, Asamura H, Ohe Y, Maeshima AM, Shibata T, Masuda N, and Matsuno Y.	Epidermal growth factor receptor mutation status and clinicopathological features of combined small cell carcinoma with adenocarcinoma of the lung.	Cancer Sci	98	1714-19	2007
Kato Y, Tsuta K, Seki K, Maeshima AM, Watanabe S, Suzuki K, Asamura H, Tsuchiya R, and Matsuno Y.	Immunohistochemical detestion of GLUT-1 can discriminate between reactive mesothelium and malignant mesothelioma.	Mod Pathol	20	215-20	2007
Nishiyama N, Yamamoto S, Matsuoka N, Fujimoto H, and Moriya Y.	Simultaneous laparoscopic descending colectomy and nephroureterectomy for descending colon carcinoma and left ureteral carcinoma: report of a case.	Surg. Today	39	728-732	2009

発表者氏名	論文タイトル名	発表誌名	巻号	ページ	出版年
Nakagawa T, Kanai Y, Komiyama M, Fujimoto H, and Kakizoe T.	Characteristics of prostate cancers found in specimens removed by radical cystoprostatectomy for bladder cancer and their relationship with serum prostate-specific antigen level.	Cancer Sci.	100	1880-1884	2009
Hinotsu S, Akaza H, Miki T, Fujimoto H, Shinohara N, Kikuchi E, Mizutani Y, Koga H, Okajima E, and Okuyama A, Japanese Urological Association.	Bladder cancer develops 6 years earlier in current smokers: analysis of bladder cancer registry data collected by the cancer registration committee of the Japanese Urological Association.	Int. J. Urol.	16	64-69	2009
Kikuchi E, Fujimoto H, Mizutani Y, Okajima E, Koga H, Hinotsu S, Shinohara N, Oya M, Miki T, and the Cancer Registration Committee of the Japanese Urological Association.	Clinical outcome of tumor recurrence for Ta, T1 non-muscle invasive bladder cancer from the data on registered bladder cancer patients in Japan: 1999-2001 report from the Japanese Urological Association.	Int. J. Urol.	16	279-286	2009

発表者氏名	論文タイトル名	発表誌名	巻号	ページ	出版年
Kakehi Y, Kamoto T, Shiraishi T, Ogawa O, Suzukamo Y, Fukuhara S, Saito Y, Tobisu K, Kakizoe T, Shibata T, Fukuda H, Akakura K, Suzuki H, Shinohara N, Egawa S, Irie A, Sato T, Maeda O, Meguro N, Sumiyoshi Y, Suzuki T, Shimizu N, Arai Y, Terai A, Kato T, Habuchi T, Fujimoto H, and Niwakawa M.	Prospective evaluation of selection criteria for active surveillance in Japanese patients with stage T1cN0M0 prostate cancer.	Jpn. J. Clin. Oncol.	38	122-128	2008
Negishi T, and Fujimoto H.	A case of locally advanced prostate cancer in the transition zone.	Jpn. J. Clin. Oncol.	38	164	2008
Shintaku I, Satoh M, Okajima E, Fujimoto H, Kamoto T, Ogawa O, Kawai K, Akaza H, Tsukamoto T, Naito S, Miki T, and Arai Y.	Survival of metastatic germ cell cancer patients assessed by international germ cell consensus classification in Japan.	Jpn. J. Clin. Oncol.	38	281-287	2008
Kamidono S, Ohshima S, Hirao Y, Suzuki K, Arai Y, Fujimoto H, Egawa S, Akaza H, Hara I, Hinotsu S, Kakehi Y, and Hasegawa T, Working Group for Creation of Clinical Practice Guidelines for Prostate Cancer, The Japanese Urological Association.	Evidence-based clinical practice Guidelines for Prostate Cancer (Summary - JUA 2006 Edition).	Int. J. Urol.	15	1-18	2008

発表者氏名	論文タイトル名	発表誌名	巻号	ページ	出版年
Miyake M, Sugano K, Kawashima K, Ichikawa H, Hirabayashi K, Kodama T, Fujimoto H, Kakizoe T, Kanai Y, Fujimoto K, Hirao Y.	Sensitive detection of FGFR3 mutations in bladder cancer and urine sediments by peptide nucleic acid-mediated real-time PCR clamping.	Biochem. Biophys. Res. Commun.	362	865-871	2007
Kouno T, Ando M, Yonemori K, Matsumoto K, Shimizu C, Katsumata N, Komiyama M, Okajima E, Matsuoka N, Fujimoto H, Fujiwara Y.	Weekly paclitaxel and carboplatin against advanced transitional cell cancer after failure of a platinum-based regimen.	Eur. Urol.	52	1115-1122	2007
Kusters M, C.J.H. van de Velde, R.G.H.Beet-Tan, Akasu T, Fujita S, Yamamoto S, Moriya Y.	Patterns of local recurrence in rectal cancer: A single-center experience.	Ann Surg Oncol	16	289-296	2009
Ishiguro S, Yamamoto S, Fujita S, Akasu T, Kasters M, Moriya Y.	Pelvic exenteration for clinical T4 rectal cancer: oncologic outcome in 93 patients at a single institution over a 30-year period.	Surgery	145 (2)	189-195	2009
Sakuraba M, Asano T, Yano T, Yamamoto S, Moriya Y.	Reconstruction of an enterocutaneous fistula using a superior gluteal artery perforator flap. (Case report)	An International Jounal of Surgical Reconstruction (JPRAS)	62	108-111	2009

発表者氏名	論文タイトル名	発表誌名	巻号	ページ	出版年
Kusters M, Beets GL, van de Velde CJ, Beets-Tan RG, Marijnen CA, Rutten HJ, Putter H, Moriya Y.	A comparison between the treatment of low rectal cancer in Japan and the Netherlands, with focus on the patterns of local recurrence.	Annals of Surgery	249 (2)	229-235	2009
Akasu T, Sugihara K, Moriya Y.	Male urinary and sexual function after mesorectal excision alone or in combination with extended lateral pelvic lymph node dissection for rectal cancer.	Ann Surg Oncol	10	2779-2786	2009
Moriya Y.	Differences in rectal cancer surgery east versus west.	Lancet Oncol	10	1026-1027	2009
Fujita S, Yamamoto S, Akasu T, Moriya Y.	Risk factors of lateral pelvic lymph node metastasis in advanced rectal cancer.	Int J Colorectal Dis	24	1085-1090	2009
Akasu T, Yamaguchi T, Fujimoto Y, Ishiguro S, Yamamoto S, Fujita S, Moriya Y.	Abdominal sacral resection for posterior pelvic recurrence of rectal carcinoma: analyses of prognostic factors and recurrence patterns.	Ann Surg Oncol	14	74-83	2007
Uehara K, Shimoda T, Nakanishi Y, Taniguchi H, Akasu T, Fujita S, Yamamoto S, Moriya Y.	Clinicopathological significance of fibrous tissue around fixed recurrent rectal cancer in the pelvis.	Br J Surg	94	1530-1535	2007

発表者氏名	論文タイトル名	発表誌名	巻号	ページ	出版年
Uehara K, Nakanishi Y, Shimoda T, Taniguchi H, Akasu T, Moriya Y.	Clinicopathological significance of microscopic abscess formation at the invasive margin of advanced low rectal cancer.	Br J Surg	94	239-243	2007
Uehara M, Yamamoto S, Fujita S, Akasu T, Moriya Y, Morisue A.	Isolated right external iliac lymph node recurrence from a primary cecum carcinoma: Report of a case.	Jpn J Clin Oncol	37(3)	230-232	2007
Nakajima T, Saito Y, Matsuda T, Hoshino T, Yamamoto S, Moriya Y, Saito D.	Minute depressed-type submucosal invasive cancer; 5mm in diameter with intermediate lymph-node metastasis. Report of a Case.	Dis Colon Rectum	50	677-681	2007
Uehara K, Yamamoto S, Fujita S, Akasu T, Moriya Y.	Impact of Upward Lymph Node Dissection on Survival Rates in Advanced Lower Rectal Carcinoma.	Dig Surg	24(5)	375-381	2007
Ishibashi Y, Yamamoto S, Yamada Y, Fujita S, Akasu T, Moriya Y	Laparoscopic resection for malignant lymphoma of the ileum causing ileocecal intussusception - Case Report-	Surg Laparosc Endosc Percutan Tech	17(15)	444-446	2007
Fujita S, Saito N, Yamada T, Takii Y, Kondo K, Ohue M, Ikeda E, Moriya Y.	Randomized, Multicenter Trial of Antibiotic Prophylaxis in Elective Colorectal Surgery.	Arch Surg	142	657-661	2007
Fujita S, Yamamoto S, Akasu T, Moriya Y, Taniguchi H, Shimoda T.	Quantification of CD10 mRNA in colorectal cancer and relationship between mRNA expression and liver metastasis.	Anticancer Research	27	3307-3311	2007
Terauchi T, Tateishi U, Maeda T, Kanou D, Daisaki H, Moriya Y, Moriyama N, Kakizoe T.	A case of colon cancer detected by carbon-11 choline positron emission tomography/ computed tomography: An initial report.	Jpn J Clin Oncol	37(10)	797-800	2007

発表者氏名	論文タイトル名	発表誌名	巻号	ページ	出版年
Yamamoto S, Fujita S, Akasu T, Ishiguro S, Kobayashi Y, Moriya Y.	Wound infection after elective laparoscopic surgery for colorectal carcinoma.	Surg Endosc	21	2248-2252	2007
Fujita S, Nakanishi Y, Taniguchi H, Yamamoto S, Akasu T, Moriya Y, Shimoda T.	Cancer invasion to Auerbach's plexus is an important prognostic factor in patients with pT3-pT4 colorectal cancer.	Dis Colon Rectum	50	1860-1866	2007
Nakagohri T, Kinoshita T, Konishi M, Takahashi S, Gotohda N, Kobayashi S, Kojima M, Miyauchi H, and Asano T	Inferior head resection of the pancreas for intraductal papillary mucinous neoplasms.	J. Hepatobiliary. Pancreat. Surg.			[Epub ahead of print]
Fujita T, Nakagohri T, Gotohda N, Takahashi S, Konishi M, Kojima M, and Kinoshita T	Evaluation of the Prognostic Factors and Significance of Lymph Node Status in Invasive Ductal Carcinoma of the Body or Tail of the Pancreas.	Pancreas			[Epub ahead of print]
Fujita T, Kojima M, Gotohda N, Takahashi S, Nakagohri T, Konishi M, Ochiai A, and Kinoshita T	Incidence, clinical presentation and pathological features of benign sclerosing cholangitis of unknown origin masquerading as biliary carcinoma.	J. Hepatobiliary. Pancreat. Surg.			[Epub ahead of print]
Shirakawa H, Suzuki H, Shimomura M, Kojima M, Gotohda N, Takahashi S, Nakagohri T, Konishi M, Kobayashi N, Kinoshita T, and Nakatsura T	Glypican-3 expression is correlated with poor prognosis in hepatocellular carcinoma.	Cancer Sci	100	1403-1407	2009

発表者氏名	論文タイトル名	発表誌名	巻号	ページ	出版年
Shirakawa H, Kuronuma T, Nishimura Y, Hasebe T, Nakano M, Gotohda N, Takahashi S, Nakagohri T, Konishi M, Kobayashi N, Kinoshita T, and Nakatsura T	Glypican-3 is a useful diagnostic marker for a component of hepatocellular carcinoma in human liver cancer.	Int. J. Oncol	34	649-656	2009
Kobayashi S, Gotohda N, Nakagohri T, Takahashi S, Konishi M, and Kinoshita T	Risk factors of surgical site infection after hepatectomy for liver cancers.	World J. Surg.	33	312-317	2009
Kinoshita T, Sasako M, Sano T, Katai H, Furukawa H, Tsuburaya A, Miyashiro I, Kaji M, and Ninomiya M	Phase II trial of S-1 for neoadjuvant chemotherapy against scirrhous gastric cancer (JCOG 0002).	Gastric Cancer	12	37-42	2009
Hirayama A, Kami K, Sugimoto M, Sugawara M, Toki N, Onozuka H, Kinoshita T, Saito N, Ochiai A, Tomita M, Esumi H, and Soga T	Quantitative metabolome profiling of colon and stomach cancer microenvironment by capillary electrophoresis time-of-flight mass spectrometry.	Cancer Res.	69	4918-4925	2009
Fujita T, Gotohda N, Takahashi S, Nakagohri T, Konishi M, and Kinoshita T	Clinical and histopathological features of remnant gastric cancers, after gastrectomy for synchronous multiple gastric cancers.	J. Surg. Oncol.	100	466-471	2009
Nobuoka D, Gotohda N, Konishi M, Nakagohri T, Takahashi S, Kinoshita T.	Prevention of postoperative pancreatic fistula after total gastrectomy.	World J. Surg.	32	2261-2266	2008

発表者氏名	論文タイトル名	発表誌名	巻号	ページ	出版年
Mitsunaga S, Kinoshita T, Hasebe T, Nakagohri T, Konishi M, Takahashi S, Gotohda N, Ochiai A.	Low serum level of cholinesterase at recurrence of pancreatic cancer is a poor prognostic factor and relates to systemic disorder and nerve plexus invasion.	Pancreas.	36	241-248	2008
Kajiwara M, Kojima M, Konishi M, Nakagohri T, Takahashi S, Gotohda N, Hasebe T, Ochiai A, Kinoshita T.	Autoimmune pancreatitis with multifocal lesions.	J. Hepatobiliary Pancreat. Surg.	15	449-452	2008
Kajiwara M, Gotohda N, Konishi M, Nakagohri T, Takahashi S, Kojima M, Kinoshita T.	Incidence of the focal type of autoimmune pancreatitis in chronic pancreatitis suspected to be pancreatic carcinoma: experience of a single tertiary cancer center.	Scand. J. Gastroenterol.	43	110-116	2008
Hasebe T, Konishi M, Iwasaki M, Nakagohri T, Takahashi A, Gotohda N, Kinoshita T, Ochiai A.	Primary tumor/vessel tumor/nodal tumor classification of extrahepatic bile duct carcinoma.	Hum. Pathol.	39	37-48	2008
Nakagohri, T., Kinoshita, T., Konishi, M., Takahashi, S., Tanizawa, Y.	Clinical Results of Extended Lymphadenectomy and Intraoperative Radiotherapy for Pancreatic Adenocarcinoma.	Hepato-Gastroenterology	54(74)	564-569	2007
Nakagohri, T., Kinoshita, T., Konishi, M., Takahashi, S., and Gotohda, N.	Surgical outcome of intraductal papillary mucinous neoplasms of the pancreas.	Ann Surg Oncol	14(11)	3174-3180	2007
Mitsunaga, S., Hasebe, T., Kinoshita, T., Konishi, M., Takahashi, S., Gotohda, N., Nakagohri, T., and Ochiai, A.	Detail Histologic Analysis of Nerve Plexus Invasion in Invasive Ductal Carcinoma of the Pancreas and Its Prognostic Impact.	Am J Surg Pathol	11(31)	1636-1644	2007
Kajiwara, M., Fujii, S., Takahashi, S., Konishi, M., Nakagohri, T., Gotohda, N., and Kinoshita, T.	Adenocarcinoma of the minor duodenal papilla with intraepithelial spread to the pancreatic duct.	Virchows Arch	451	1075-1081	2007

発表者氏名	論文タイトル名	発表誌名	巻号	ページ	出版年
Kajiwara, M., Gotohda, N., Konishi, M., Nakagohri, T., Takahashi, S., Kojima, M., Hasebe, T., and Kinoshita, T.	Cystic endocrine tumor of the pancreas with an atypical multilocular appearance.	J Hepatobiliary Pancreat Surg	14	586-589	2007
Sano T.	Adjuvant and neoadjuvant therapy of gastric cancer: a comparison of three pivotal studies.	Current Oncol. Rep.	10	191-198	2008
Sasako M, Sano T, Yamamoto S, Kurokawa Y, Nashimoto A, Kurita A, Hiratsuka M, Tsujinaka T, Kinoshita T, Arai K, Yamamura Y, Okajima K: Japan Clinical Oncology Group.	D2 lymphadenectomy alone or with para-aortic nodal dissection for gastric cancer.	N. Engl. J. Med.	359	453-462	2008
Morita S, Katai H, Saka M, Fukagawa T, Sano T, Sasako M.	Outcome of pylorus-preserving gastrectomy for early gastric cancer.	Br. J. Surg.	95	1131-1135	2008
Oda I, Gotoda T Sasako M, Sano T, Katai H, Fukagawa T, Shimoda T, Emura F, Saito D.	Treatment strategy after non-curative endoscopic resection of early gastric cancer.	Br. J. Surg.	95	1495-1500	2008
Nunobe S, Sano T.	Symptom evaluation of long-term postoperative outcomes after pylorus-preserving gastrectomy for early gastric cancer.	Gastric Cancer	10	167-172	2007
Kosaka Y, Sano T.	Identification of the high-risk group for metastasis of gastric cancer cases by vascular endothelial growth factor receptor-I overexpression in peripheral blood.	British J Cancer	96	1723-1728	2007
Sano T.	Tailoring treatments for curable gastric cancer.	Br J Surg	94	263-264	2007

発表者氏名	論文タイトル名	発表誌名	巻号	ページ	出版年
Sasako M, Sano T.	Surgical treatment of advanced gastric cancer: Japanese perspective.	Dig Surg	24	101-107	2007
Tsujinaka T, Sano T.	Influence of overweight on surgical complications for gastric cancer: results from a randomized control trial comparing D2 and extended para-aortic D3 lymphadenectomy (JCOG9501).	Ann Surg Oncol	14	355-361	2007

Radiol Phys Technol (2008) 1:44–54
DOI 10.1007/s12194-007-0008-8

Experimental verification of proton beam monitoring in a human body by use of activity image of positron-emitting nuclei generated by nuclear fragmentation reaction

Teiji Nishio · Aya Miyatake · Kazumasa Inoue · Tomoko Gomi-Miyagishi · Ryosuke Kohno · Satoru Kameoka · Keiichi Nakagawa · Takashi Ogino

Received: 2 July 2007 / Revised: 22 October 2007 / Accepted: 23 October 2007 / Published online: 27 November 2007

Abstract Proton therapy is a form of radiotherapy that enables concentration of dose on a tumor by use of a scanned or modulated Bragg peak. Therefore, it is very important to evaluate the proton-irradiated volume accurately. The proton-irradiated volume can be confirmed by detection of pair-annihilation gamma rays from positron-emitting nuclei generated by the nuclear fragmentation reaction of the incident protons on target nuclei using a PET apparatus. The activity of the positron-emitting nuclei generated in a patient was measured with a PET-CT apparatus after proton beam irradiation of the patient. Activity measurement was performed in patients with tumors of the brain, head and neck, liver, lungs, and sacrum. The 3-D PET image obtained on the CT image showed the visual correspondence with the irradiation area of the proton beam. Moreover, it was confirmed that there were differences in the strength of activity from the PET-CT images obtained at each irradiation site. The values of activity obtained from both measurement and calculation based on the reaction cross section were compared, and it was confirmed that the intensity and the distribution of the activity changed with the start time of the PET imaging after proton beam irradiation. The clinical use of this information about the positron-emitting nuclei will be important for promoting proton treatment with higher accuracy in the future.

Keywords Proton therapy · Proton beam monitoring · Beam OFF-LINE PET system · PET-CT imaging

T. Nishio (✉) · T. Gomi-Miyagishi · R. Kohno · S. Kameoka · T. Ogino
Particle Therapy Division, Research Center for Innovative Oncology, National Cancer Center, Kashiwa,
6-5-1 Kashiwano-ha, Kashiwa-shi, Chiba 277-8577, Japan
e-mail: tnishio@east.ncc.go.jp

T. Nishio · A. Miyatake
Department of Nuclear Engineering and Management, Graduate School of Engineering, University of Tokyo,
2-11-16 Yayoi, Bunkyo-ku, Tokyo 113-0032, Japan

T. Nishio · K. Nakagawa
Department of Radiology, Graduate School of Medicine, University of Tokyo, 7-3-1 Hongo, Bunkyo-ku,
Tokyo 113-8655, Japan

K. Inoue
Department of Radiology, National Cancer Center, Kashiwa,
6-5-1 Kashiwano-ha, Kashiwa-shi, Chiba 277-8577, Japan

Present Address:
K. Inoue
Functional Imaging Division, Research Center for Innovative Oncology, National Cancer Center, Kashiwa,
6-5-1 Kashiwano-ha, Kashiwa-shi, Chiba 277-8577, Japan

K. Inoue
Graduate School of Health Science, Tokyo Metropolitan University, 7-2-10 Higashiogu, Arakawa-ku,
Tokyo 116-8551, Japan

1 Introduction

Proton therapy has allowed the dose to be concentrated only on a tumor. The use of proton therapy is spreading throughout the world as a highly accurate method of radiation therapy [1]. In the future, proton therapy will be expected to become one of the main forms of radiation therapy because of its high utility. On the other hand, the diagnosis of an initial or small tumor has become

possible with developments in imaging methods that provide high resolution and contrast. In particular, positron emission tomography (PET) has advanced rapidly, and its use has become widespread. PET-computed tomography (CT) combines PET and CT and is now readily available. The fusion of PET and CT images can be achieved with high precision by use of a PET-CT apparatus. As a result, the location of activity can be determined with high accuracy.

In this study, the activity of positron-emitting nuclei generated by the nuclear fragmentation reaction of incident protons and nuclei constituting of a patient body was measured with a PET-CT apparatus (beam OFF-LINE PET system), and the proton-irradiated volume was confirmed. So far most researches were limited to phantom studies using a PET apparatus (no combined with CT apparatus) [2–13]. Verification of activity measurement was performed in patients with tumors of the brain, head and neck, liver, lungs, and sacrum. By use of a fusion imaging obtained with a combined PET-CT apparatus, the irradiated volume was confirmed immediately after proton therapy with higher accuracy than that the use of fusion of images obtained from the separate PET apparatus and CT apparatus.

We are researching dose-volume delivery-guided proton therapy (DGPT) for confirmation of the proton-irradiated volume and dose distribution by using a beam ON-LINE PET system (BOLPs) in the proton treatment room [13]. The activity image of each treatment site obtained with the PET-CT apparatus will be used for the simulation and estimation of the activity image acquired from the BOLPs immediately after proton irradiation to a patient.

This paper is organized as follows. Experimental procedures are described in Sect. 2. Measurement and analysis results and discussion are presented in Sect. 3. Section 4 discusses the conclusions of this study regarding proton therapy.

2 Materials and methods

2.1 Nuclear fragmentation reaction of incident protons and target nuclei

The nuclear fragmentation reaction occurs in the human body by high-energy proton beam irradiation during proton therapy. Many kinds of nuclei, including positron-emitting nuclei, are generated by the reaction.

The activity $N_{\beta+}$ of the positron-emitting nuclei Y generated from each type of tissue composition by the nuclear fragmentation reaction is expressed as the following equation [11]:

$$\begin{aligned} &N_{\beta+}(tissue;E_p)\,[\mathrm{kBq/cc/GyE}] \\ &= \Phi_p(tissue;E_p) \\ &\cdot \sum_X \sum_Y \left| \begin{array}{l} \frac{1}{T_m}\cdot\left\{1-\exp\left(-\sigma_{X\to Y}(E_p)\cdot n_{tissue}(X)\cdot\Delta_{tissue}\right)\right\} \\ \times\left\{\frac{T_{1/2}(Y)}{T_i\cdot\ln 2}\cdot\left(1-2^{-T_i/T_{1/2}}(Y)\right)\right\} \\ \times 2^{-T_0/T_{1/2}}(Y)\times\left(1-2^{-T_m/T_{1/2}}(Y)\right) \end{array} \right|, \end{aligned} \tag{1}$$

Here, X denotes the target nuclei in the tissue, z the depth, T_m the time of the activity measurement, T_i the time of the proton irradiation, T_0 the interval between the start of the activity measurement and the discontinuation of proton irradiation, and $T_{1/2}$ the half life of the generated positron-emitting nuclei. The reaction cross section of $\sigma_{X\to Y}$, which determines the rate of generation in the nuclear fragmentation reaction $X(p,x)Y$, depends on the kind of target nucleus (mass number A_t, atomic number Z_t) and the relative kinetic energy of E_p. n_{tissue} denotes the number per unit volume of the nucleus in the tissue, and Δ_{tissue} the target thickness. Data of human body composition are based on ICRU Report 46 [14]. The number of incident protons per the dose and the volume Φ_p, is expressed as follows:

$$\begin{aligned} &\Phi_p(tissue;E_p)\,[\mathrm{protons/cc/GyE}] \\ &= 1\times10^{-3}\Big/\left\{\left(dE_p/dx[\mathrm{J/cm}]\right)\cdot RBE\right\} \\ &= \left[1.671\times10^{-11}\cdot\left\{\frac{\ln\left(1.363\times10^4\cdot\left(\gamma(E_p)^2-1\right)\right)}{\beta(E_p)^2}-1\right\}\right]^{-1}. \end{aligned} \tag{2}$$

Here, RBE is the relative biological effectiveness. β and γ are expressed by use of the kinetic energy of the proton, in the following equation:

$$\begin{aligned} &\beta(E_p)=\sqrt{1-\frac{1}{\left(1+1.066\times10^{-3}\cdot E_p\right)^2}}, \\ &\gamma(E_p)=1+1.066\times10^{-3}\cdot E_p. \end{aligned} \tag{3}$$

The ^{12}C, ^{14}N, ^{16}O, and ^{40}Ca nuclei are main chemical elements of the human body [14]. For proton therapy, the number of each positron-emitting nuclei, generated in the human body depends on the target nuclei and on the incident proton beam energy.

Some the experimental data of the reaction for $^{12}C(p,x)Y$, $^{14}N(p,x)Y$, $^{16}O(p,x)Y$ have been reported [15]. The mean values of the reaction cross sections of the ^{11}C, ^{13}N, and ^{15}O nuclei generated from the ^{12}C and ^{16}O nuclei are especially expressed as follows [11]:

$$\sigma_{X\to Y}(E_p) = \frac{a}{1+\exp\left(\frac{b-E_p}{c}\right)} \cdot \left\{1 - d\cdot\left(1 - e\cdot\exp\left(-\frac{E_p - f}{g}\right)\right)^h\right\},$$

$$\begin{bmatrix} X & Y & a & b & c & d & e & f & g & h \\ {}^{12}C & {}^{11}C & 96.0 & 21.4 & 0.9 & 0.5 & 1.2 & 39.0 & 34.5 & 2.0 \\ {}^{16}O & {}^{15}O & 71.0 & 26.0 & 2.8 & 0.6 & 1.1 & 41.0 & 36.0 & 6.0 \\ {}^{16}O & {}^{13}N & 66.0 & 10.4 & 0.4 & 0.9 & 0.8 & 11.6 & 6.8 & 1.0 \\ {}^{16}O & {}^{11}C & 18.8 & 43.6 & 3.6 & 0.5 & 1.0 & 49.0 & 35.0 & 4.0 \end{bmatrix}. \quad (4)$$

Here, the reaction cross section of $\sigma_{X\to Y}$ and the relative kinetic energy E_p have units of mb and MeV, respectively. The letters a, ..., h are constant parameters for the calculation of the reaction cross section in each reaction channel. The data of the reaction for $^{40}Ca(p,x)Y$ is mainly calculated with the INTENSITY code [16, 17] because there is no experiment value.

2.2 Proton therapy at each treatment site

The proton radiotherapy facility of the National Cancer Center, Kashiwa has a small normal-conducting AVF cyclotron (C235) for medical purposes, two rotating gantry ports, and one horizontal fixed port [18, 19]. For obtaining laterally uniform irradiation fields, the dual-ring double scattering method is used in one rotating gantry port and the horizontal fixed port; the wobbler method is used with the other rotating port. The uniform proton dose distribution during proton treatment is controlled by a simple feed back control system equipped with an automatic fine adjustment of the beam axis and a mechanism for moving the second dual-ring scatter of the double scatters to the optimal position [20]. Using this system, we achieved uniform dose distribution in the irradiation field during proton radiotherapy, with symmetry within ±1% and flatness within 2%. The accuracy of the calculated dose is similarly proportional to the accuracy of the measured and calculated activities.

Verification of the activity measurement was performed in about 20 cases with tumors of the brain, head and neck, liver, lungs, and sacrum. Proton beam irradiation to the liver and lung was performed with synchronization to the respiratory motion of the target organ. The position uncertainty of the target organ is within 5 mm. The proton treatment planning system, PTPLAN/ndose, developed in our facility [21] was used for planning of the proton treatment. The accuracy of the proton range is estimated within 3 mm in conversion of Hounsfield units (HU) of the planning CT image to water equivalent length. The accuracy of the dose calculation will be within 5% for the homogeneous or simply inhomogeneous body (e.g., prostate, liver, lung), and be greater than 10% at the boundary of the inhomogeneous tissue (e.g., head and neck). The dose calculation was performed with the margin of the 3 mm for the brain and the head and neck, and 5 mm for the liver, the lung, and the prostate.

2.3 Measurement of activity with PET-CT apparatus

The activity of the positron-emitting nuclei generated in the patients by proton beam irradiation was measured with the PET-CT apparatus (Discovery ST (GE Medical Systems, Milwaukee, Wisconsin, U.S.A.)) at our institution. The PET-CT apparatus was a detection system with 10,080 BGO (Bismuth-Germanium-Oxide) with a crystal size of 6.2 × 6.2 × 30 mm^3 arranged on a circumference of a circle with a diameter of 88.6 cm. 3D reconstruction algorithm of OSEM (Ordered Subsets Expectation Maximization) was employed with a position resolution of 5.0–6.7 mm, which was position-dependent. The axial size of the field of view (FOV) was 15.7 cm. The accuracy of the absolute activity measured with the commercial PET-CT apparatus has been reported to be commonly about 10% [22].

The distance between the room for proton treatment and the room with the PET-CT apparatus was about 40 m. Therefore, PET scanning was started about 7 min after irradiation, and the image was acquired over 5 min. Therefore, the biological washout effect in the metabolism of a living tissue is important for the verification of the absolute activity and the activity distribution of the positron-emitting nuclei induced by the proton irradiation. In studies in which the radioactive ion beam (^{11}C,^{10}C) to a rabbit was irradiated, the decay curve has three components of a fast decay (decay constant ~2–10 s), medium decay (decay constant ~100–200 s), and slow decay (decay constant ~3,000–10,000 s) [23, 24]. The 50–65% of total activity is the fast and medium components.

The proton beam was irradiated to the tumor in the liver and lungs with the beam synchronized to respiratory motion. However, the activity of the positron-emitting nuclei generated in the patient was measured without synchronizing to respiratory motion of the target organ. The corresponding tumor movement will be a few cm.

3 Results and discussion

3.1 Visual verification of PET-CT image at each treatment site

The measured activity distribution and the calculated dose distribution on CT image for proton treatment of a tumor in the sacrum as one of the site studies are shown in Fig. 1. Proton beam irradiation was performed with a gantry angle of 180 degrees and a dose of 2.5 GyE [= [Gy] x *RBE* (= 1.1 = constant)]. Moreover, the width of the spread-out Bragg peak (SOBP) was 70 mm. The activity fitted on the area of proton irradiation was visually confirmed by comparison with the proton dose distribution. The activity observed in the proton irradiated area of subcutaneous adipose tissue and bone tissue was higher than that in the surrounding area.

Figure 2 shows the results for prostate tumor. Proton beam irradiation was performed with a gantry angle of 90°, a SOBP width of 60 mm, and a dose of 2.0 GyE. Similarly, high activity was observed in the subcutaneous adipose tissue and in the femur.

Figure 3 shows the results for a tumor of the head and neck. Proton beam irradiation was performed twice with each dose of 2.0-GyE, and a gantry angle of 230° for the initial exposure, followed by 330° for the second one. The respective widths of the SOBP were 80 and 70 mm. The interval between the two irradiation procedures was about 9 min. Therefore, the activity of the 330° proton beam was higher than that of the 230° beam. High activity was similarly observed in the areas of adipose tissue and maxilla irradiated by the proton beam.

Figure 4 shows the results for a liver tumor. Proton beam irradiation was performed with a 3.8-GyE dose and 80 mm SOBP from a gantry angle of 290°. During treatment, the proton beam irradiation was synchronized to the respiratory motion of the target organ. However, during the acquisition of PET-CT image data, there was no synchronization to the respiratory motion. Similarly, high activity was observed in the area of subcutaneous adipose tissue. The findings of activity during proton treatment after a transarterial chemoembolization therapy (TACE) procedure using lipiodol for a liver tumor are shown in Fig. 5. The CT value of 80–350 HU in area including the lipiodol is considerably higher than 70 HU in a normal liver. Proton beam irradiation was performed with a 3.8-GyE dose and 80 mm SOBP at a gantry angle of 180°. The activity in the liver tumor was high. We speculated that this was because many positron-emitting nuclei were generated from the iodine nuclei contained in the lipiodol.

3.2 Specificity of activity generated in each body tissue

The activity in each tissue and the interval between beam-stop time and start-time of activity measurement was calculated from Eq. 1. A beam irradiation time of 2 min and the beam energy in each tissue are used in the calculation. The reaction cross sections of $^{12}C(p,x)^{11}C$, $^{16}O(p,x)^{15}O$, $^{16}O(p,x)^{13}N$, and $^{16}O(p,x)^{11}C$ reactions were calculated from Eq. 4 at each proton energy. The reaction cross sections of $^{12}C(p,x)^{10}C$, $^{16}O(p,x)^{14}O$, $^{40}Ca(p,x)^{38}K$, $^{40}Ca(p,x)^{30}P$, $^{40}Ca(p,x)^{15}O$, $^{40}Ca(p,x)^{13}N$, and $^{40}Ca(p,x)^{11}C$ reactions were calculated with the INTENSITY code. For

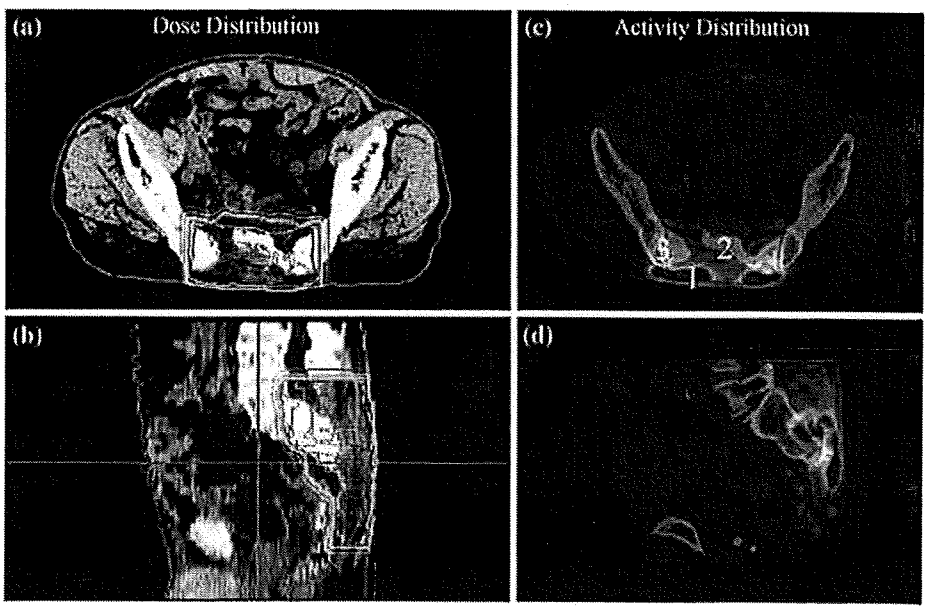

Fig. 1 Dose distribution calculated with the proton treatment planning system and activity measured with the PET-CT apparatus on CT image after proton treatment of tumor in the sacrum. The iso-dose line of 100% is red, 80% yellow green, 50% light blue, and 20% purple. The activity line of 5 kBq/cc is red, 3 kBq/cc green, and 1 kBq/cc bule. Proton beam irradiation was performed with an SOBP of 70 mm, gantry angle of 180°, and dose of 2.5 GyE. The dose distributions on each CT image in axial and coronal planes are shown in figures (**a**) and (**b**), and the activity are shown in figures (**c**) and (**d**)

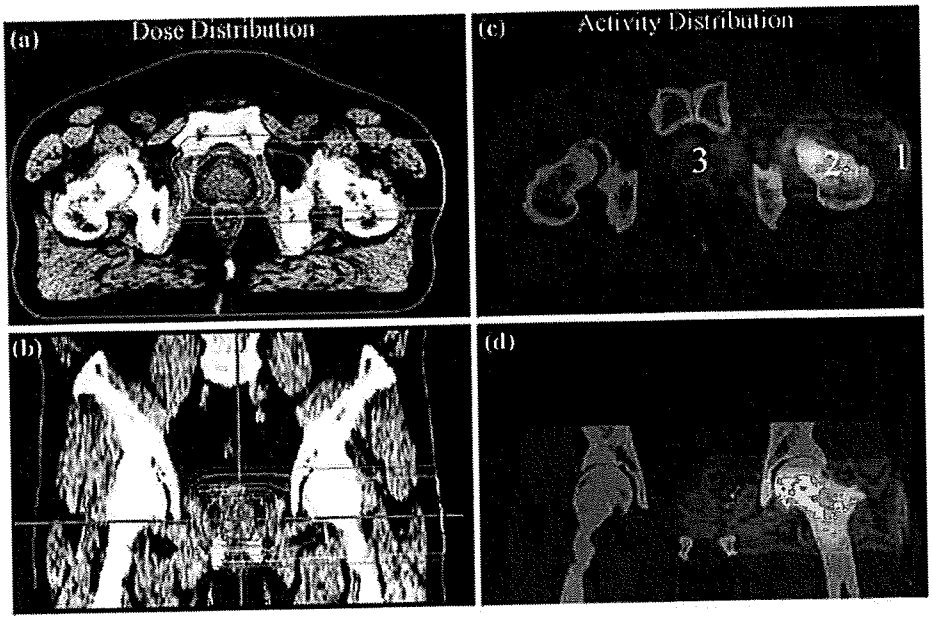

Fig. 2 Dose distribution calculated with the proton treatment planning system and activity measured with the PET-CT apparatus on CT image after proton treatment of tumor in the prostate. The iso-dose line of 100% is red, 80% yellow green, 50% light blue, and 20% purple. The activity line of 5 kBq/cc is red, 3 kBq/cc green, and 1 kBq/cc bule. Proton beam irradiation was performed with an SOBP of 60 mm, gantry angle of 90°, and dose of 2.0 GyE. The dose distributions on each CT image in axial and coronal planes are shown in figures (**a**) and (**b**), and the activity are shown in figures (**c**) and (**d**)

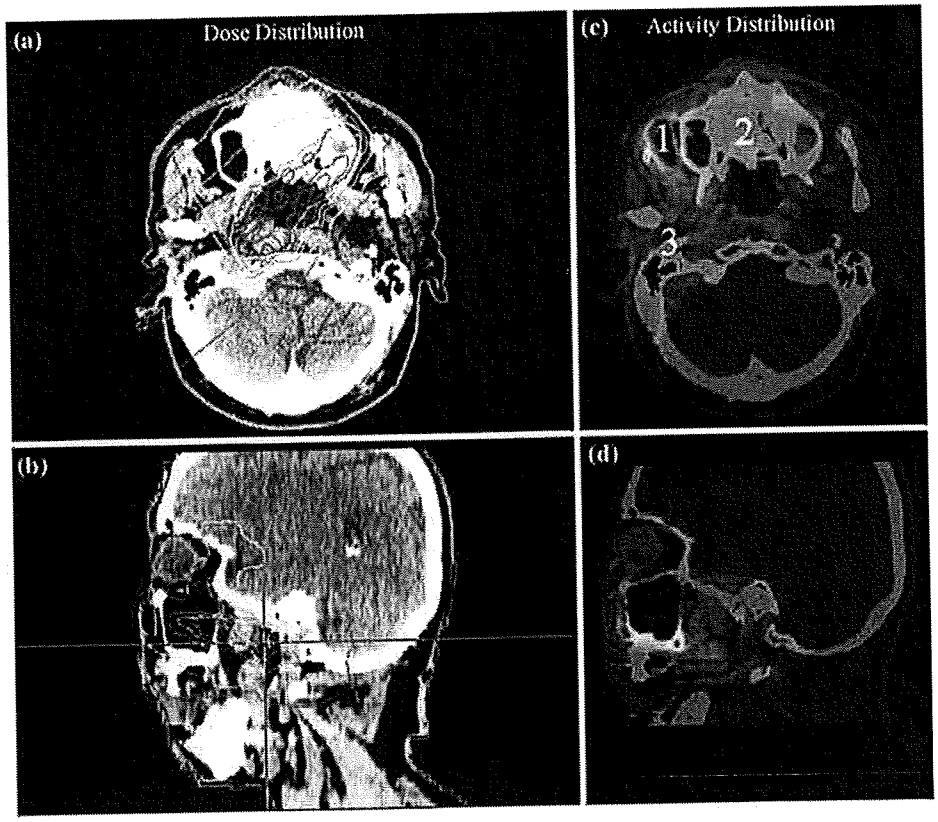

Fig. 3 Dose distribution calculated with the proton treatment planning system and activity measured with the PET-CT apparatus on CT image after proton treatment of tumor in the head and neck. The iso-dose line of 100% is red, 80% yellow green, 50% light blue, and 20% purple. The activity line of 5 kBq/cc is red, 3 kBq/cc green, and 1 kBq/cc bule. Proton beam irradiation was performed with an SOBP of 70 mm, gantry angle of 330°, and dose of 2.0 GyE after irradiation with an SOBP of 80 mm, gantry angle of 230°, and dose of 2.0 GyE. The dose distributions on each CT image in axial and coronal planes are shown in figures (**a**) and (**b**), and the activity are shown in figures (**c**) and (**d**)

$^{14}N(p,x)^{13}N$, $^{14}N(p,x)^{11}C$, and $^{14}N(p,x)^{10}C$ reactions, experimental data [15] were used. The results are shown in Fig. 6. Data of each human body composition and the proton energy used for the calculation of the time dependent activity in various tissues are shown in Table 1. The activity of adipose tissue was higher than that in the liver more than 6 min after proton beam irradiation. The same tendency was shown for activity measurements with use of the PET-CT apparatus after proton treatment for liver cancer.

The calculated decay curve is approximated with two components of short (^{15}O, ^{14}O, ...) and long (^{13}N, ^{11}C, ...) half life, and is expressed as the following equation:

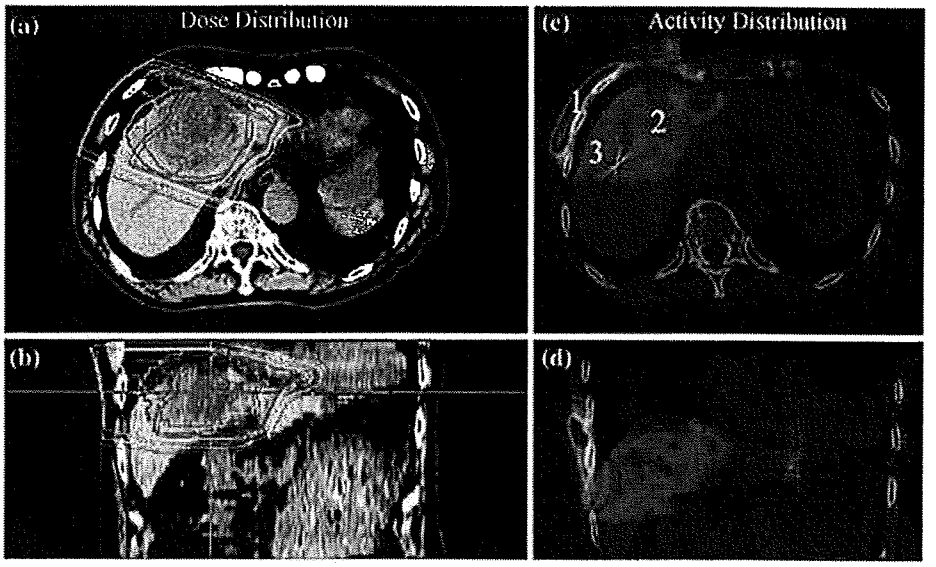

Fig. 4 Dose distribution calculated with the proton treatment planning system and activity measured with the PET-CT apparatus on CT image after proton treatment of tumor in the liver. The iso-dose line of 100% is red, 80% yellow green, 50% light blue, and 20% purple. The activity line of 7 kBq/cc is red, 5 kBq/cc green, and 3 kBq/cc bule. The proton beam irradiation was performed with an SOBP of 80 mm, gantry angle of 290°, and dose of 3.8 GyE. The dose distributions on each CT image in axial and coronal planes are shown in figures (a) and (b), and the activity are shown in figures (c) and (d)

$$N_{\beta+}(Tissue;T_0)[\mathrm{kBq/cc/GyE}] = \begin{cases} 2.2\times 2^{-T_0[\mathrm{min}]/1.9}+0.6\times 2^{-T_0[\mathrm{min}]/17.7} & (\mathrm{Tumor}) \\ 3.1\times 2^{-T_0[\mathrm{min}]/2.0}+0.5\times 2^{-T_0[\mathrm{min}]/16.8} & (\mathrm{Liver}) \\ 1.4\times 2^{-T_0[\mathrm{min}]/1.9}+0.8\times 2^{-T_0[\mathrm{min}]/18.6} & (\mathrm{Adipose\ Tissue}) \\ 5.9\times 2^{-T_0[\mathrm{min}]/2.0}+1.6\times 2^{-T_0[\mathrm{min}]/17.8} & (\mathrm{Skeleton\ Cranium}) \\ 3.0\times 2^{-T_0[\mathrm{min}]/1.9}+1.4\times 2^{-T_0[\mathrm{min}]/17.8} & (\mathrm{Skeleton\ Femur}) \\ 4.3\times 2^{-T_0[\mathrm{min}]/1.9}+1.3\times 2^{-T_0[\mathrm{min}]/17.4} & (\mathrm{Skeleton\ Ribs}) \end{cases} \quad (5)$$

The value of short or long half life in each tissues was consistent within 5% accuracy, and was equal to the our study using a dead rabbit [13]. This result showed that the activity at $T_0 = 0$ (condition of the measurement in the BOLPs) was higher five times than that at $T_0 = 7$ min (condition of this work in the commercial PET-CT apparatus).

Figure 7 shows the ratio R of the calculated activity normalized to one at $T_0 = 0$. It is expressed as the following equation:

$$R(tissue;T_0) = \frac{N_{\beta+}(Tumor;T_0=0)}{N_{\beta+}(Tissue;T_0=0)} \cdot \frac{N_{\beta+}(Tissue;T_0)}{N_{\beta+}(Tumor;T_0)}. \quad (6)$$

The results showed that the image of the activity changed during $T_0 = 0 \sim 10$ min. Therefore, the observed image of off-line PET (commercial PET-CT apparatus) will be different from that of the on-line PET (BOLPs).

The value of the activity at points 1, 2, and 3 on the axial activity images are shown in Figs. 1, 2, 3, 4 and 5. The points were selected on the soft tissue (tumor), the subcutaneous adipose tissue, and the bone tissue. The reaction cross sections, the kinetic energies of the proton beam at each point, and the half lives of the positron-emitting nuclei are shown in Table 2. The irradiation dose, irradiation time, interval between discontinuing the beam and acquiring the PET image, and the measured, the calculated value (Calculation: B) and the differences of activity at the point are summarized in Table 3.

It was estimated that the measured activity had a statistical accuracy of 9% (2 kBq/cc at 10 cm path length in the human body, 5 min measurement, each cubic voxel with a perimeter of 4 mm), and the image reconstruction accuracy was 10%. The accuracy of the measured activity in the biological washout effect is estimated to be very large, and is difficult to show the correspondence quantitatively. Moreover, the coefficient of the effect is always smaller than one. In the calculated activity, the accuracy of the reaction cross sections and the number of incident protons were estimated to be 20 and 5%, respectively. In the soft tissue and the liver, the measurement and the calculation activity were consistent within the error bar. On the other hand, the measured activity was about two to four times as large as the calculated activity in the adipose tissue, and about two times that in the femur. In the high activity of the adipose tissue, the accuracy of the attenuation correction factor of the 511-keV gamma ray based on the CT value of the subcutaneous adipose tissue under the adjacent body surface will partly influence the discrepancy in the activity measurement. The high activity of the femur was probably due to the accuracy of the calculation based on the fragmentation reaction cross section of ^{40}Ca. In the liver tumor after a TACE procedure with lipiodol, the measured activity was about four times as large as the calculated activity in the case without the lipiodol. It is noted that the nuclear fragmentation reaction of the iodine contained in the lipiodol is unknown well.